frontiers | Frontiers in Imaging

TYPE Original Research
PUBLISHED 21 November 2023
DOI 10.3389/fimag.2023.1133311

Check for updates

OPEN ACCESS

EDITED BY
Quan Wang,
Chinese Academy of Sciences (CAS), China

REVIEWED BY
Karissa Beth Tilbury,
University of Maine, United States
Kiril Alexiev,
Institute of Information and Communication Technologies (BAS), Bulgaria

*CORRESPONDENCE
Magdalena Stocker
magdalena.widmann91@gmail.com

RECEIVED 28 December 2022
ACCEPTED 26 October 2023
PUBLISHED 21 November 2023

CITATION
Stocker M, Baumeister P, Canis M, Vogel M and Gires O (2023) Second harmonic generation imaging of head and neck squamous cell carcinoma. *Front. Imaging.* 2:1133311. doi: 10.3389/fimag.2023.1133311

COPYRIGHT
© 2023 Stocker, Baumeister, Canis, Vogel and Gires. This is an open-access article distributed under the terms of the Creative Commons Attribution License (CC BY). The use, distribution or reproduction in other forums is permitted, provided the original author(s) and the copyright owner(s) are credited and that the original publication in this journal is cited, in accordance with accepted academic practice. No use, distribution or reproduction is permitted which does not comply with these terms.

Second harmonic generation imaging of head and neck squamous cell carcinoma

Magdalena Stocker[1]*, Philipp Baumeister[1], Martin Canis[1], Martin Vogel[2] and Olivier Gires[1]

[1]Department of Otorhinolaryngology, Head and Neck Surgery, Ludwig-Maximilians-University Munich, Munich, Germany, [2]BIOPTec Technical Engineering and Prototyping, Max-Planck-Institutes of Biophysics, Frankfurt, Germany

Head and neck squamous cell carcinomas (HNSCC) are a heterogenous group of tumors with a poor prognosis and treatments impairing the patients' quality of life. We assessed post-surgical human head and neck squamous cell carcinomas (HNSCC) and healthy tissue ($n = 10$ each) via HHG (higher harmonic generation) imaging to differentiate healthy from tumor tissue. Qualitative imaging analysis compared collagen fibrils detected via immunohistology and SHG (second harmonic generation). Quantitative analysis measured the forward to backward intensity ratio (f_{SHG}/b_{SHG}) of SHG images. Assessments of the tissue samples demonstrated a structural difference of collagen matrix organization from healthy to malignant tissue. Healthy tissue was characterized by a high f/b ratio, describing highly organized tissue, whereas a low f/b ratio was observed in malignant tissue, indicative of reduced organization. Properly distinguishing tumor from healthy tissue is crucial to a successful treatment and best possible outcome for the individual patient. SHG provides broad possibilities to analyze extracellular changes in diseased tissue, such as solid tumors and to distinguish tumor from healthy tissue.

KEYWORDS

non-linear optics, multiphoton microscopy, second harmonic generation imaging, head and neck squamous cell carcinoma, extracellular matrix

1 Introduction

Head and neck squamous cell carcinomas (HNSCC) are a heterogenous group of tumors of the lips, mouth, salivary glands, inner nose, pharynx and larynx (Sung et al., 2021). Approximately 700,000 people worldwide are diagnosed with HNSCC each year, making it the sixth most common cancer worldwide (Ferlay et al., 2015). The 5-year-survival rate is 51% (men) and 61% (women), the 10-year-survival rate drops to 39% in men and 50% in women. Tobacco use of any kind and alcohol consumption are considered to be the main risk factors for the development of HNSCC and especially cancer of the mouth, hypopharynx, and larynx (Blot et al., 1988; Winn et al., 2015). Another more recently defined risk factor is a chronic infection with human papillomavirus (HPV) strains, especially type 16 of the high risk group (Argiris et al., 2008; Marur et al., 2010). A central aspect of HNSCC that impacts most strongly on prognosis is the frequent formation of nodal metastases and a strong tendency of these tumors to recur during cancer progression (van Houten et al., 2004). Tumor cell dissemination and metastases formation is supported by a transcriptional re-programming known as partial epithelial-to-mesenchymal transition (p-EMT) (van Houten et al., 2004), the detachment of single or few malignant cells from tumor areas resulting in so-called tumor budding, and a high degree of therapy resistance of disseminated cells (Leemans et al., 2018; Pierik et al., 2021). Hence, specific and sensitive detection of minimal residual disease (MRD) in the process of HNSCC diagnosis may improve the patients' outcome.

Furthermore, patients frequently suffer from therapeutical consequences that have a relevant impact on the quality of life. Since these tumors occur in a region that is highly functional, surgical as well as irradiation-based therapies are often associated with a substantial functional impairment. The loss of physiological phonation in laryngectomies, loss of sense of smell and taste, dysphagia, dysphonia, xerostomia due to surgical interventions and radiation therapy, as well as cosmetic impairments are relevant consequences patients are confronted with (Nelke et al., 2014). Hence, properly distinguishing tumor and normal tissue is of crucial clinical importance as it may minimize the risk of residual tumor tissue in surgical resection on the one hand and, on the other hand, may avoid removing an unnecessarily large amount of healthy tissue surrounding the tumor that creates further functional impairments. The purpose of the present work was to use laser scanning Second Harmonic Generation (SHG) imaging to examine tissue samples from HNSCC and corresponding healthy tissue of patients to investigate whether SHG can help differentiate healthy tissue of the head and neck region from HNSCC.

SHG is a nonlinear optic phenomenon: two photons (in practice with a wavelength of typically $\geq$ 800 nm) are coherently scattered at the extracellular collagen matrix of the tissue to generate a higher harmonic photon with half of the wavelength (Provenzano et al., 2006; Burke et al., 2013). Thus, a multiplication of the frequency occurs, the formation of so-called harmonics. The term higher harmonic generation (HHG) summarizes these nonlinear optic effects, including SHG and also third harmonic generation (THG), that emerges from three photons generating a single photon with a third of the original wavelength (Helmchen and Denk, 2005). In contrast to linear optics, the wavelength of the emitted light changes. A change of the wavelength due to nonlinearity enables a representation of certain structures in the range of visible wavelengths (Aptel et al., 2010). The prerequisite for non-linear optics is a high light intensity generated by a pulsed laser (Dela Cruz et al., 2010). The coherence of the incoming with the outgoing light distinguishes SHG from fluorescence. In fluorescence, molecules of the irradiated matter are excited unlike in SHG imaging. The energy that reaches the tissue is essentially not absorbed by it and thus no energy exchange occurs. Phototoxicity as well as bleaching effects of the tissue can be significantly lower than, for example, with fluorescence microscopy (Campagnola and Loew, 2003; Zipfel et al., 2003; Green et al., 2017). In addition, due to the laser wavelength in the near infrared range, a penetration depth of several hundred micrometers is achievable (Campagnola et al., 2002; Campagnola and Loew, 2003). SHG is a second-order nonlinear optical process that has symmetry constraints confining signal to regions lacking a center of symmetry (Campagnola et al., 2002; Helmchen and Denk, 2005). It can image variations in the extracellular matrix (ECM) as it emerges from non-centrosymmetric structures such as several collagen types (Campagnola et al., 2002; Tilbury and Campagnola, 2015). The sub-resolution fibrillar assembly is revealed through emission directionality. This information is inherent to the tissue's symmetrical properties due to the coherence and phase-matching process of SHG. Measurements of SHG emission directionality, *i.e.* forward to backward propagating SHG signal (f/b ratio), can give information on structural changes in tissue and enable a differentiation between healthy and tumor tissue (Nadiarnykh et al., 2010). The f/b ratio depends on fibril diameter and packing density, *i.e.* order and disorder in fibril packing as well as the amount of collagen in the respective tissue (LaComb et al., 2008; Burke et al., 2013). THG provides information on cell-cell as well as cell-collagen matrix integrity and visualizes cells as well as membrane borders (Adur et al., 2011).

The tumor microenvironment contains all cellular and non-cellular structures surrounding the tumor, including immune cells, fibroblasts, blood and lymph vessels, and also the ECM (Venning et al., 2015). Alteration of the microenvironment can lead to facilitation of tumor progression and metastasis, including an altered and dynamic composition of the ECM and collagen that can be seen in malignant tumors (Zhu et al., 1995; Kauppila et al., 1998). Components of the ECM such as collagen not only have support and stability functions but are also involved in signaling pathways, cell migration, and other processes (Rozario and DeSimone, 2010; Walker et al., 2018). Alteration of ECM and more specifically collagen type I has been found to influence cell invasion in malignant tumors (Sapudom et al., 2015; Chen et al., 2019). Hence, a closer look at these structures provides deepened insights regarding carcinogenesis, growth, and metastasis (Cox and Erler, 2011). It is reasonable to state that tumor invasion and metastasis are facilitated by altered ECM (Venning et al., 2015). ECM is therefore of great diagnostic interest with respect to malignant diseases and broadens the view of the dynamics and scope of changes in malignant growth.

2 Materials and methods

2.1 Tissue samples and preparation

Tissue samples from ten patients with HNSCC [oropharyngeal (n = 2) and hypopharyngeal (n = 8) cancer] were examined. Regions with tumor-growth as well as healthy tissue were analyzed. Post-surgical tissue samples were snap-frozen, embedded in O.C.T compound (optimal cutting temperature, TissueTek® O.C.T compound, Sakura Finetek, USA) and cut with a cryotome into four µm thick samples. The samples were prepared for immunohistological staining and *Elastica van Gieson* staining. The antibody used for immunohistology was specific for collagen-I-type (Abcam, ab21286, concentration: 100 µl at 1.71 mg/ml, 1:100) and was combined with a biotinylated anti-mouse-antibody as secondary antibody (Abcam, ab64255, concentration: 100 µl at 7 µg/ml, 1:100). Light microscopy was utilized for analysis [Leica DMi8 microscope, Leica, Wetzlar, Germany, Contrasting methods: (transmitted light base) TL BF, TL PH, TL POL, IL FLUO; objectives: 5x: N PLAN 5x/0.12 PH0, 10x: HC PI. FLUOTAR 10x/0.32 PH1, 20x: HC PI. FI. I. 20x/0.40 CORR PH1, 40x: HC PI. FLUOTAR I. 40x/0.60 CORR PH2; condenser: Turret: BF, PH1, PH0 (no polarizer), IL-Turret (Filter

Abbreviations: ECM, extracellular matrix; HHG, higher harmonic generation; HNSCC, head and neck squamous cell carcinoma; MT-MMP, membrane type matrix metalloproteinase; OCT, optimal cutting temperature; OPO, optic parametric oscillator; SHG, second harmonic generation; THG, third harmonic generation; TPEF, two-photon excited fluorescence microscopy.

cube): DAPI, FITC, TXR, EMP_BF; software: LAS X Premium with 1TB SSD RAID, camera: Leica DFC3000 g, light source: CoolLED pE300 lite]. Consecutive slides of the samples were stained only with hemalum and analyzed via SHG imaging. Qualitative imaging analysis compared collagen matrices detected via immunohistology and SHG. Quantitative imaging analysis measured forward to backward intensity ratio (f_{SHG}/b_{SHG}) of SHG images. The setting of the project is described in Figure 1.

The project was in accordance with the ethical standards of the Institutional Ethics Committee (project 140-13) and with the 1964 Helsinki declaration and its later amendments or comparable ethical standards.

2.2 Multiphoton microscopy

A TriM Scope, a multiphoton microscopy platform (La Vision Biotec, Bielefeld, Germany), combined with an Olympus BX51 microscope (Olympus, Hamburg, Germany), and a pulsed femtosecond Titanium/Sapphire laser (Coherent, Dieburg, Germany) was used. The laser generates wavelengths between 500 nm and 900 nm. Additionally, an OPO (optic parametric oscillator, typical pulse width 200 fs, repetition rate 80 MHz, pumped by the Ti:Sa-Laser) (APE, Berlin, Germany) was used to generate wavelengths up to 1,300 nm to create THG of cells and cell borders. The laser beams were focused onto the sample with an Olympus 20x/0.95 W objective, which offers a working distance of two millimeters. The following detection channels were used: backward (epi) detection (417–477 nm), forward detection (417–477 nm). 700 nm short pass filters blocked out excitation light. Light collection in forward direction was performed by an Olympus WI-UCD condenser, NA 0.8. Photomultiplier tubes (PMTs) were Hamamatsu H6780-01. The setup of detectors as well as intensity and wavelengths of the laser were kept constant during all experiments to assure comparable results in each tissue sample.

2.3 Data acquisition

Data was analyzed with the software FIJI ("FIJI Is Just Image J"). FIJI is a freely accessible software for data analysis (Schindelin et al., 2012). F/b ratios of all tissue samples were generated with FIJI. Two different regions were chosen in every tissue sample. Furthermore, within these regions, two regions of interest (ROI) from each tissue sample were chosen, based on the highest pixel intensity i.e., the highest amount of collagen. Pixel intensity in the ROI and each of the two regions of the respective tissue samples was measured. Threshold application and further image analysis was performed as follows: as a first step, a minimal threshold intensity signal in the background of each sample (500 μm^2) was manually selected and substracted from the sample (Aaron and Chew, 2021). Then, the ROI was chosen (200–300 μm^2). Images were then converted into 32-bit. Forward directed images were then divided by the backward directed images. The values were then logarithmized. To avoid that dominant F values are weighted more compared to large B values, log (F/B) values have been computed.

3 Results

3.1 Collagen fibrils in conventional immunohistology vs. SHG

Coll-I immunohistological staining were compared with SHG to evaluate a specific visualization of collagen fibrils. The goal was to verify the SHG signal as a specific method to visualize non-centrosymmetric collagen fibrils, mainly collagen type 1. This has already been shown in different experiments by various research groups in other tumor entities (Williams et al., 2005; Rivard et al., 2014; Tilbury and Campagnola, 2015). An established method for the histological interpretation of collagenous tissue was used as a baseline for the visualization of collagen in the tissue samples. The different samples were each stained in immunohistology with coll-1-specific antibodies for light microscopical analysis. Consecutive sections were stained with *Elastica van Gieson* staining for further light microscopical analysis of collagen and furthermore with hemalum for multiphoton microscopy. Even though histological staining is no prerequisite for image analysis via SHG, the tissue was stained for better orientation and subsequent identification of the areas of interest. Identical areas that appeared collagen-rich in immunohistology were visualized on the multiphoton microscope. Thus, a direct comparison was conducted in consecutive tissue slides.

It was found that collagen type 1 stained by immunohistology was also visible as SHG signal within the corresponding tissue area.

SHG signals in Figure 2 do not originally appear as a magenta-colored signal but are colored subsequently with the software FIJI to enable an easier visual interpretation of the signal. Cells were visualized via THG, which was used in this project to create a holistic image of the tissue samples and are colored in green in the right panel of Figure 2. SHG and THG signals were created separately from each other since different wavelengths were used for those different signals (SHG $\geq$ 800 nm, THG $\geq$ 1,200 nm, wavelength elongation for THG with an OPO). The separate images were merged and colored via FIJI subsequently, creating a comparable microscopical image to allow to judge the congruence to the immunohistological image. It is important to note that THG was not further included in the experiments. THG was incorporated to serve as a visual, to create a holistic view of the tissue and to facilitate comparison of the different imaging techniques.

3.2 Forward to backward intensity ratio

Two separate images were taken of each of the areas analyzed with the multiphoton microscope: one reflecting the forward propagated and one representing the backward propagated signal. Figure 3 shows f_{SHG} and b_{SHG} in healthy tissue and HNSCC. The f/b ratio depends on fibril diameter and packing density, *i.e.* order and disorder in fibril packing as well as the amount of collagen in the respective tissue (Burke et al., 2013).

Two separate regions of interest (ROI) of 500 x 500 µm in each tissue sample were examined. In each original image, the section with the most intense SHG signal with maximum amount

10.3389/fimag.2023.1133311

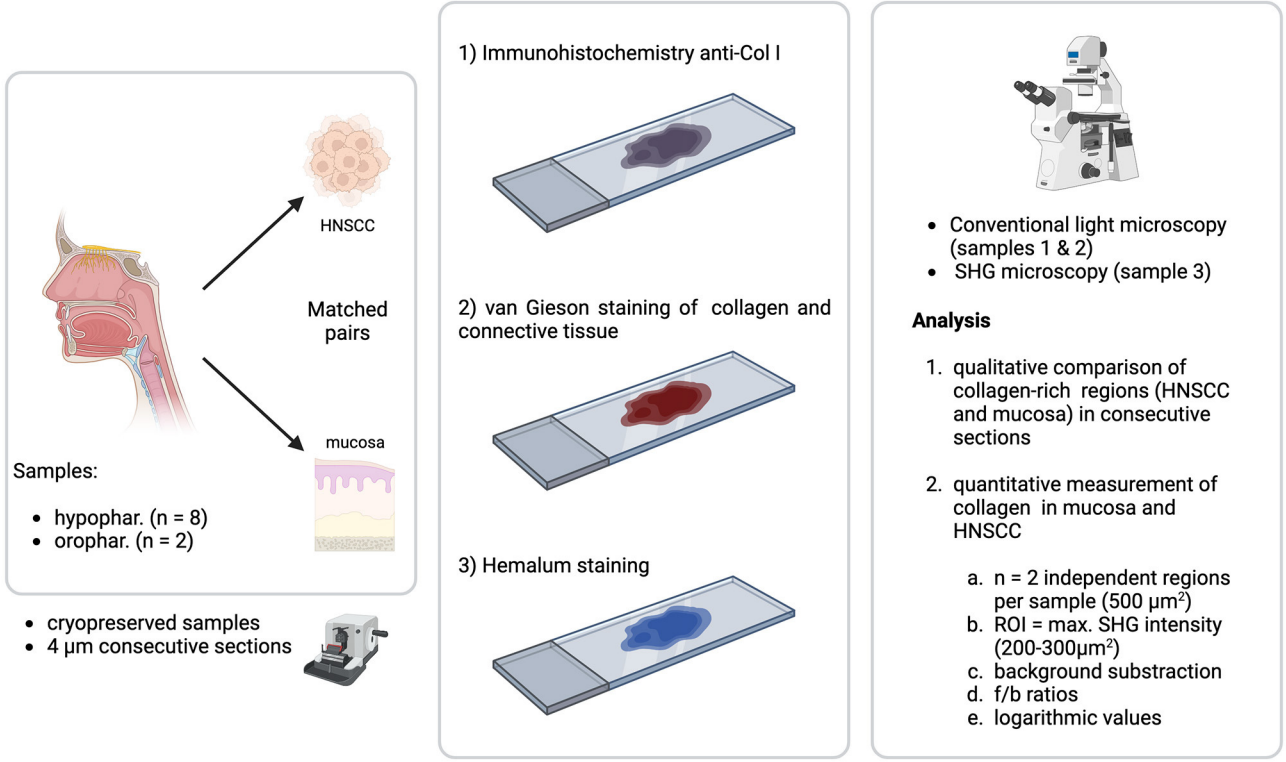

FIGURE 1
Setting of the project. Cryoconserved samples (4 µm consecutive sections) of matched pairs (tumor and healthy mucosa) of 10 tumor samples from HNSCC (hypopharynx $n = 8$, oropharynx $n = 2$) were stained with immunohistochemistry anti-col 1, Elastica van Gieson staining and hemalum. Samples 1 and 2 (immunohistochemistry and Elastica van Gieson) were analyzed with a light microscope, sample 3 (hemalum) with a multiphoton microscope. Image analysis consisted of two parts: (1) Qualitative comparison of collagen-rich regions (HNSCC and mucosa) in consecutive sections and (2) Quantitative measurement of collagen in mucosa and HNSCC. The second part of image analysis was performed on each two independent regions (500 μm^2). A ROI with the maximum SHG intensity of 200–300 μm^2 was chosen for analysis via f/b-ratio after threshold application and logarithmization of the values.

of collagen of optimized organization was consistently selected as the region of interest to achieve the greatest possible comparability. This section was between 200 x 200 and 300 x 300 µm large. It was composed of numerous pixel values that are individually scanned by the lasers of the multiphoton microscope. The pixel values are to be regarded as independent individual values, with the information of several thousand pixels being contained in one ROI, providing detailed image information. All these steps were performed for all healthy mucosal samples as well as for tumor samples. Thus, 40 different f/b ratios were calculated, two from each tissue sample. Those two results from each tissue sample were totaled. The tissue samples were directly compared as matched pairs, meaning every healthy tissue sample was compared with HNSCC from the same patient. Finally, after averaging, 20 f/b ratios were compared in two data sets as boxplots for healthy tissue and HNSCC (Figure 4). Differences of the f/b-ratio between healthy mucosa and tumor areas were analyzed for statistical significance with a two-sample t-test assuming different variances. With a p-value of 0.04610027, the differences between the f/b-ratio in tumor tissue vs. healthy tissue were significant. The assessment of the tissue samples demonstrated a structural change of collagen matrix organization from healthy to malignant tissue. Eight out of ten matched pairs showed a higher f/b ratio in healthy tissue than in the corresponding HNSCC. Only two out of ten samples showed a higher f/b ratio in HNSCC. These two samples (4 and 5) showed no differences from the other samples with respect to the localization of the tumor. They were, respectively, oropharyngeal and hypopharyngeal carcinomas. Samples 1, 2 and 5 were hypopharyngeal tumor samples, samples 3 and 6–10 were oropharyngeal tumor samples.

Hence, the presented method, namely measurement of f/b ratio in SHG images of healthy tissue and HNSCC can outline significant differences between those types of tissue in terms of changes in collagen fibrils. The information obtained can be used to broaden the diagnostic as well as therapeutic possibilities for HNSCC.

4 Discussion

SHG allows detailed imaging of non-centrosymmetric structures such as fibrillar collagen, myosin and microtubules (Tilbury and Campagnola, 2015). It is a tissue-sparing technique with a low risk of phototoxicity or bleaching of the tissue, as occurs with other techniques such as two-photon excitation microscopy (TPEF) (Campagnola and Loew, 2003; James and Campagnola, 2021). The foundation of signal collection is the symmetry property of the structures of interest; thus, no staining

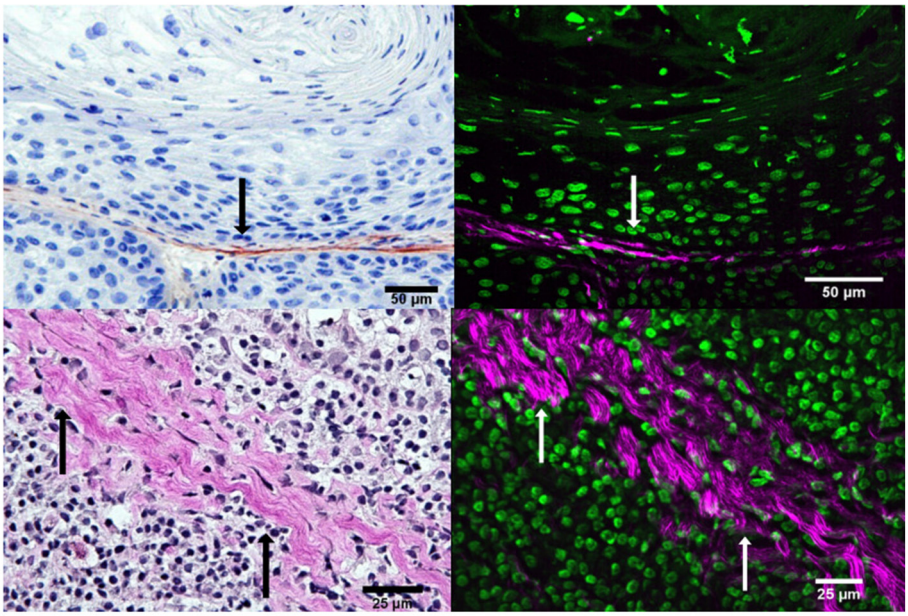

FIGURE 2
Comparison of collagen fibrils in coll-1 immunohistology **(upper left)** and van Gieson **(lower left)** with SHG+THG **(right)** of consecutive slides of tumor tissue showing the size bar (50 µm and 25 µm). On the **upper left** i.e., the immunohistological slide, collagen is shown in brown, nuclei and cytoplasm in blue. On the **lower left** i.e., the van Gieson slide, collagen is shown in magenta, nuclei in black, cytoplasm in light brown. On the **right**, collagen is shown as SHG signal in magenta, cell nuclei and cytoplasm as THG signal in green. Arrows in black and white mark similar structures in the images.

of the tissue is required (Campagnola et al., 2002; Campbell and Campagnola, 2017).

The tissue images obtained by the multiphoton microscope represent forward propagated and backward propagated signals. These are the result of two detectors that receive different information: the forward signal f_{SHG} contains the photons that have passed through the tissue and reached the detector behind the tissue. The backward signal b_{SHG} is a result of quasi-phase matching of the SHG process (LaComb et al., 2008). Most tissues have a certain degree of irregularity of collagen fibers, packing density and fibril diameter that might even increase in diseased states and thus have an impact on phase matching processes and therefore the generated backward signal b_{SHG} (LaComb et al., 2008). The randomness in biological tissue has an impact on the different SHG signals (LaComb et al., 2008). Both signals, f_{SHG} and b_{SHG} provide important information about the arrangement and quantity of collagen fibrils in the tissue.

In this study, all analyzed tumor samples were p16 negative epithelial tumors. Oropharyngeal and hypopharyngeal squamous cell carcinoma have a similar histopathological and molecular structure, if p16 negative, as is in this study. For HPV-negative SCC, the two most frequent genomic alterations are *p53* (83%) and *CDKN2A* (57%) according to The Cancer Genome Atlas (TCGA) data (Cancer Genome Atlas Network, 2015; Leemans et al., 2018). That is for oropharyngeal and hypopharyngeal cancer.

P16 positive HNSCC have a relevant difference in molecular pathological structure (Leemans et al., 2018). None of the tumor samples in this study had an association with HPV. Since all patients in this study were smokers, an association with nicotine consumption and tumor initiation is debatable. Tobacco use of any kind and alcohol consumption are considered to be the main risk factors for the development of HNSCC and especially cancer of the mouth, hypopharynx, and larynx (Helmchen and Denk, 2005; Han and Brown, 2010; Green et al., 2017).

All patients had a pathological T2 or T3 staging, thus a comparable tumor size and, overall, the patient collective was homogenous, despite the origin of cancer varying from hypopharynx to oropharynx. That supports the theory of the two tumor samples with a different f/b-ratio being possible statistical outliers. Though it needs to be discussed, whether the chosen method of selecting ROIs might have an influence on the measured f/b-ratio. ROIs were selected based on identifying collagen-rich areas in the immunohistological slides that had a certain recognition value, like an easily identifiable arrangement of collagen strands in the tissue. But the amount of collagen in tumor might vary due to remodeling processes in the tissue. However, the chosen measurement protocol more likely mimics the clinical routine and was thus chosen herein.

Changes in the ECM are highly relevant regarding the development and progression of malignant neoplasms (Brown et al., 2003; Nadiarnykh et al., 2010; Cox and Erler, 2011; Burke et al., 2013). ECM as a part of the tumor microenvironment plays a vital role in the initiation and progression of malignant cells in tissue (Venning et al., 2015). An altered composition of the ECM in general and specifically collagen is observed in malignant tumors (Zhu et al., 1995; Kauppila et al., 1998; Ramaswamy et al., 2003; Lu et al., 2012). However, these changes are diverse: desmoplasia i.e., an increase in the amount of collagen

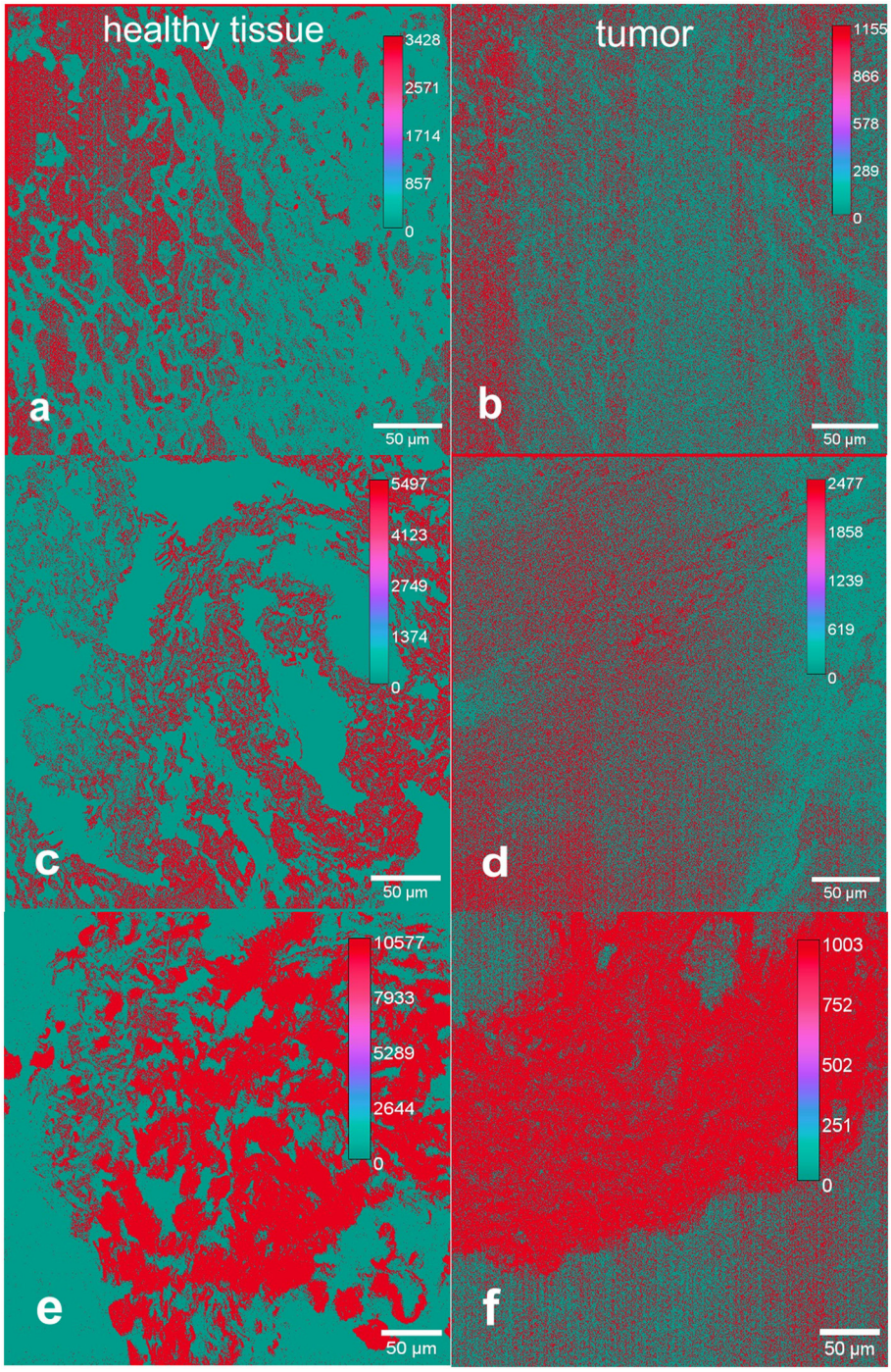

FIGURE 3
Forward to backward intensity ratios of SHG signals in healthy [left, **(a, c, e)**] and tumor [right, **(b, d, f)**] tissue from the head and neck region. Shown are representative examples including size bars (50 µm). The color scaled pixel intensity is indicated in each representative image. The ratio from forward to backward propagated signals is higher in healthy tissue compared to tumor tissue. This is indicated by the maximum pixel intensity amounts of the respective tissue samples in healthy tissue and tumor.

(Pupa et al., 2002; Tilbury et al., 2014) but also a decreased amount of collagen compared to healthy tissue (Curino et al., 2005; Wolf et al., 2007) and also an increased cross-linking of fibrils (Levental et al., 2009) have been reported. These changes can be summarized under the term remodeling (Adur et al., 2014). Remodeling in malignant degenerated tissue serves to facilitate tumor progression and invasion. Numerous structures are involved in this process, including enzymes such as metalloproteinases, which are capable of degrading highly stable type 1 collagen as well as other collagens (Hotary et al., 2000; Friedl and Gilmour, 2009). It is suggested

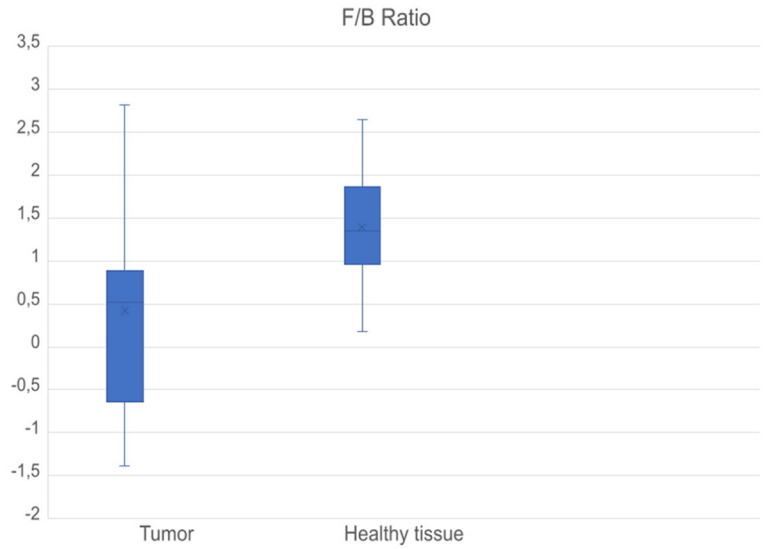

FIGURE 4
Boxplots comparing f/b ratios of all tumor samples **(left)** and healthy samples **(right)**. Mean values of the respective f/b ratios of all tissue samples in healthy and tumor tissue were taken into consideration. Values are logarithmized, a value of −1 means a value lower by one power of ten, and a value of 1 means a value higher by one power of ten.

that membrane-type matrix metalloproteinases (MT-MMPs) can mediate proteolytic processes within the ECM to disrupt collagen I rich membrane barriers and thus facilitate tumor invasion (Adur et al., 2014).

Due to the great heterogeneity of solid tumors, it is conceivable that collagen fibrils do not behave in the same way in every tumor. They may serve as an invasion path for tumor cell dissemination in some tumors due to high linearity of the fibers (Friedl and Wolf, 2008). Fibers arranged in a linear and sometimes radial fashion around the solid tumor have been found in certain tumor entities, particularly breast carcinomas (Provenzano et al., 2006; Conklin et al., 2011). Collagen fibers arranged radially around tumor cells have also been described as a risk factor for invasiveness in head and neck tumors as demonstrated by Conklin et al. demonstrated using HNSCC cell lines with high invasiveness (OECM-1 and SAS). Spheroids of these cell lines were embedded and cultured in 3D collagen type I matrices containing fluorescent particles. Fluorescence microscopy over time revealed a radial arrangement of collagen fibrils around the tumor cell spheroids (Conklin et al., 2011).

Increased amounts of collagen fibrils in tumor tissue have also been observed and described as a factor for tumor invasiveness (Provenzano et al., 2008). Provenzano et al. demonstrated a significantly higher risk of developing breast carcinomas as well as pulmonary metastases in Col1a1tmJae-mutated mouse models. These mice carry a mutation in the region of a matrix metalloproteinase for collagen type I and are thus resistant to enzymatic degradation of collagen type I. Col1a1tmJae-mutated mice thus developed excessive collagen production. These mouse models showed a 2.5-fold increase in stromal collagen compared with wild-type models (Provenzano et al., 2008). Mouse models with this mutation showed not only higher rates of invasive tumors, but also higher rates of pulmonary metastases (Provenzano et al., 2008).

However, degradation of fibers to facilitate invasion by epithelial tumors has also been observed. Curino et al. demonstrated this using uPARAP/Endo180, a member of the macrophage mannose receptor family of endocytic transmembrane glycoproteins. Here, higher expression of uPARAP/Endo180 by mesenchymal cells was described in regions of active tissue transformation such as tumor tissue. Thus, the surrounding stroma of tumor tissue increases the expression of uPARAP/Endo180, and increased expression of uPARAP/Endo180 promotes lysosomal degradation of collagen. This was demonstrated in a comparative mouse model using mammary carcinoma-developing, uPARAP/Endo180-deficient, and wild-type mice. In tumors of the uPARAP/Endo180-deficient mouse models, collagen continued to be detectable extracellularly over the course of several hours. In the non-deficient model, collagen was detectable in intracellular vesicles (Curino et al., 2005). Lysosomal degradation of collagen is considered here to be an important aspect of collagen reduction in tumor tissue for further tumor progression. With the knowledge that components of the ECM such as collagens not only have support and stability functions, but are involved in signaling pathways, cell migration, and other processes (Rozario and DeSimone, 2010; Walker et al., 2018), they are also coming to the forefront with respect to understanding malignant events.

A comprehensive understanding of all aspects involved in tumor progression is necessary to make diagnosis and therapy of malignancies as successful as possible. HHG imaging and with it SHG is a promising and useful tool for imaging and interpreting altered ECM in human tissue. Several research groups have already shown that reliable conclusions can be made to distinguish between several solid tumor entities and healthy tissue. Examinations of

human ovarial tissue *ex vivo* presented a higher f/b ratio of SHG-signals in healthy tissue compared to ovarian cancer (Nadiarnykh et al., 2010), which is in line with the findings presented here. Changes of F/b-ratios of SHG-signals dependent on the grading of different ovarian tumors (from benign, to low-grade invasive and high-grade invasive) (Campbell and Campagnola, 2017) or type of ovarian tissue (normal ovarian tissue, benign tumors, low and high grade serous ovarian cancer, low grade endometrioid cancer) were detectable (Tilbury et al., 2017). Furthermore, a study comparing human breast cancer tissue with *carcinomata in situ* and healthy mammarian tissue *ex vivo* described a significantly higher f/b ratio in healthy compared to breast cancer tissue (Burke et al., 2013). The decreased f/b ratio of SHG signals from HNSCC samples in this project and other human tissue samples in the referred publications suggests that collagen fibrils in malignant tissue are more disordered in their structure, decreased in their amount, or both. A high f/b ratio indicates a strong forward signal resulting from a high order of fibrils and/or abundant collagen in the tissue, a low f/b ratio, respectively, the opposite (Han and Brown, 2010; Chen et al., 2012; Tilbury and Campagnola, 2015). The rationale is that the more ordered and linear collagen fibrils occur in tissue, the greater the f_{SHG}/b_{SHG} is due to less scattering of photons (Ajeti et al., 2011). This means that only a small fraction of the emitted photons is scattered and reflected by collagen fibrils. With the assumption that tumor tissue is not subject to controlled growth, a low f/b ratio can be expected here consequently.

The possibility to differentiate between healthy tissue and malignant tumor via HHG broadens the diagnostical options as presented here in HNSCC. Functional preservation is directly associated with quality of life after surgical resection of head and neck tumors. Through detailed and reliable assessment of tumor resection margins, therapy can be performed with maximum sparing of healthy tissue and potentially increased detected of MRD. This makes it easier to achieve functional preservation without increasing the risk of residual tumor cells *in situ*. Intravital imaging techniques such as HHG enable a compatibility of oncologic safety and functional preservation by specifically differentiating between healthy and malignant tissue. They allow the analysis of not only cellular but also extracellular changes in diseased tissue.

Regarding HNSCC, *in vivo* interpretation of tumor margins is relevant considering the possibility of residual tumor masses *in situ*. Long-term exposition of tissue with alcohol and cigarette smoke is a risk factor for field cancerization, an appearance of precancerous lesions in the vicinity of the primary tumor first described by Slaughter et al. (1953). These lesions are often clinically indistinguishable from healthy tissue unless they present with overt dysplasia. Leukoplakia, mucosal atrophies, or even completely unremarkable clinical findings adjacent to the tumor may be seen, which however harbor molecular changes associated with a pre-malignant state (Pierik et al., 2021). Failure to resect these premalignant lesions leads to a high recurrence rate of the tumor and thus a poor prognosis (Poh et al., 2006; Ryser et al., 2016). The tissue-protecting properties of HHG allow *in vivo* applications (James and Campagnola, 2021). Tissue samples do not need to be stained and can be analyzed microscopically directly after resection. Microscopy in the sense of frozen section diagnostics would be conceivable, which could make valid statements about a resection *in sano* or a possibly necessary more radical resection directly in the intraoperative setting. Research groups have already examined resection margins of colon carcinomas in this way and were able to detect significant differences between tumor-free and tumor-involved resection margins (Yan et al., 2014). Equally conceivable would be an application complementary to frozen section diagnostics to allow direct intraoperative *in vivo* detection of the required extent of tissue resection using HHG microscopy. This would require a compact microscope suitable for an operating room and a standardized analysis capability of the respective tumor to make valid statements (Meyer et al., 2013).

Another promising development concerning *in vivo* diagnostics via HHG is endoscopic microscopy (Ducourthial et al., 2015; Williams and Campagnola, 2015; Zhang et al., 2019). Coupled to existing fiber optic imaging devices or as a completely independent multiphoton micro-endoscope, these tools could enhance pathology analysis of multiple diseases including HNSCC and allow real-time surgical determination of tumor margins intraoperatively (Wu et al., 2009; Zhang et al., 2012).

Changes of the ECM as detected via f/b ratio might even present as a diagnostic marker for HNSCC. To establish a reliable diagnostical tool, higher patient numbers have yet to be evaluated with this method in retrospective and prospective cohorts with clinical follow-up.

5 Summary and conclusion

Our results support the theory of highly disordered collagen in malignant tumors—here in particular HNSCC—compared to healthy tissue. These structural changes were made visible by SHG. Multiphoton microscopy, and with it SHG, are promising tools for the diagnosis of malignant diseases. Tumor diagnostics and therapy could be performed in a more targeted and tissue-sparing manner. This part of non-linear optics is a dynamic field of research with highly interesting findings in recent years. It can provide information on different tissue structures on its own and create a holistic, detailed image of the respective tissue when combined with other imaging techniques. The move toward tissue-sparing, minimally invasive types of microscopy opens a broad field in the diagnosis of a wide variety of diseases with potential implications in therapeutic choices. The potential of non-linear optics in medicine has already been demonstrated in recent years and will be further exploited with future development of clinical application areas.

Data availability statement

The original contributions presented in the study are included in the article/Supplementary material, further inquiries can be directed to the corresponding author.

Ethics statement

The studies involving humans were approved by Ethics Committee of Ludwig-Maximilians-University Munich, Germany, Project 140-13. The studies were conducted in accordance with the

local legislation and institutional requirements. The participants provided their written informed consent to participate in this study.

Author contributions

MS acquired and analyzed data, created figures, and wrote the manuscript. MV analyzed data and wrote the manuscript. PB, MC, and OG created figures and wrote the manuscript.

Acknowledgments

The authors thank Christian Pfeffer for initial support at the multiphoton microscope.

Conflict of interest

The authors declare that the research was conducted in the absence of any commercial or financial relationships that could be construed as a potential conflict of interest.

The author(s) MC declared that they were an editorial board member of Frontiers, at the time of submission. This had no impact on the peer review process and the final decision.

Publisher's note

All claims expressed in this article are solely those of the authors and do not necessarily represent those of their affiliated organizations, or those of the publisher, the editors and the reviewers. Any product that may be evaluated in this article, or claim that may be made by its manufacturer, is not guaranteed or endorsed by the publisher.

Supplementary material

The Supplementary Material for this article can be found online at: https://www.frontiersin.org/articles/10.3389/fimag.2023.1133311/full#supplementary-material

References

Aaron, J., and Chew, T.-L. (2021). A guide to accurate reporting in digital image processing - can anyone reproduce your quantitative analysis? *J. Cell. Sci.* 134:jcs254151. doi: 10.1242/jcs.254151

Adur, J., Pelegati, V. B., de Thomaz, A. A., Baratti, M. O., Andrade, L. A., Carvalho, H. F., et al. (2014). Second harmonic generation microscopy as a powerful diagnostic imaging modality for human ovarian cancer. *J. Biophotonics.* 7, 37–48. doi: 10.1002/jbio.201200108

Adur, J. F., Pelegati, V. B., Costa, L. F. L., Pietro, L., Thomas, A. A., d., et al. (2011). Recognition of serous ovarian tumors in human samples by multimodal nonlinear optical microscopy. *J. Biomed. Opt.* 16, 1–10. doi: 10.1117/1.3626575

Ajeti, V., Nadiarnykh, O., Ponik, S. M., Keely, P. J., Eliceiri, K. W., Campagnola, P. J., et al. (2011). Structural changes in mixed Col I Col V collagen gels probed by SHG microscopy, implications for probing stromal alterations in human breast cancer. *Biomed. Opt. Express* 2, 2307–2316. doi: 10.1364/BOE.2.002307

Aptel, F., Olivier, N., Deniset-Besseau, A., Legeais, J.-., M., Plamann, K., et al. (2010). Multimodal nonlinear imaging of the human cornea. *Invest. Ophthalmol. Vis. Sci.* 51, 2459–2465. doi: 10.1167/iovs.09-4586

Argiris, A., Karamouzis, M. V., Raben, D., and Ferris, R. L. (2008). Head and neck cancer. *Lancet* 371, 1695–1709. doi: 10.1016/S0140-6736(08)60728-X

Blot, W. J., McLaughlin, J. K., Winn, D. M., Austin, D. F., Greenberg, R. S., Preston-Martin, S., et al. (1988). Smoking and drinking in relation to oral and pharyngeal cancer. *Cancer Research* 48, 3282–3287.

Brown, E., McKee, T., diTomaso, E., Pluen, A., Seed, B., Boucher, Y., et al. (2003). Dynamic imaging of collagen and its modulation in tumors in vivo using second-harmonic generation. *Nat. Med.* 9, 796–800. doi: 10.1038/nm879

Burke, K., Tang, P., and Brown, E. (2013). Second harmonic generation reveals matrix alterations during breast tumor progression. *J. Biomed. Opt.* 18, 31106. doi: 10.1117/1.JBO.18.3.031106

Campagnola, P. J., and Loew, L. M. (2003). Second-harmonic imaging microscopy for visualizing biomolecular arrays in cells, tissues and organisms. *Nat. Biotechnol.* 21, 1356–1360. doi: 10.1038/nbt894

Campagnola, P. J., Millard, A. C., Terasaki, M., Hoppe, P. E., Malone, C. J., Mohler, W. A., et al. (2002). Three-dimensional high-resolution second-harmonic generation imaging of endogenous structural proteins in biological tissues. *Biophys J.* 82, 493–508. doi: 10.1016/S0006-3495(02)75414-3

Campbell, K. R., and Campagnola, P. J. (2017). Assessing local stromal alterations in human ovarian cancer subtypes via second harmonic generation microscopy and analysis. *J. Biomed. Opt.* 22, 1–7. doi: 10.1117/1.JBO.22.11.116008

Cancer Genome Atlas Network (2015). Comprehensive genomic characterization of head and neck squamous cell carcinomas. *Nature* 517, 576–582. doi: 10.1038/nature14129

Chen, X., Nadiarynkh, O., Plotnikov, S., and Campagnola, P. J. (2012). Second harmonic generation microscopy for quantitative analysis of collagen fibrillar structure. *Nat Protoc.* 7, 654–669. doi: 10.1038/nprot.2012.009

Chen, Y.-Q., Kuo, J.-C., Wei, M.-T., Chen, Y.-C., et al. (2019). Early stage mechanical remodeling of collagen surrounding head and neck squamous cell carcinoma spheroids correlates strongly with their invasion capability. *Acta. Biomater.* 84, 280–292. doi: 10.1016/j.actbio.2018.11.046

Conklin, M. W., Eickhoff, J. C., Riching, K. M., Pehlke, C. A., Eliceiri, K. W., Provenzano, P. P., et al. (2011). Aligned collagen is a prognostic signature for survival in human breast carcinoma. *Am. J. Pathol.* 178, 1221–1232. doi: 10.1016/j.ajpath.2010.11.076

Cox, T. R., and Erler, J. T. (2011). Remodeling and homeostasis of the extracellular matrix: implications for fibrotic diseases and cancer. *Dis Model Mech.* 4, 165–178. doi: 10.1242/dmm.004077

Curino, A. C., Engelholm, L. H., Yamada, S. S., Holmbeck, K., Lund, L. R., Molinolo, A. A., et al. (2005). Intracellular collagen degradation mediated by uPARAP/Endo180 is a major pathway of extracellular matrix turnover during malignancy. *J. Cell. Biol.* 169, 977–985. doi: 10.1083/jcb.200411153

Dela Cruz, J. M., McMullen, J. D., Williams, R. M., and Zipfel, W. R. (2010). Feasibility of using multiphoton excited tissue autofluorescence for in vivo human histopathology. *Biomed. Opt. Express.* 1, 1320–1330. doi: 10.1364/BOE.1.001320

Ducourthial, G., Leclerc, P., Mansuryan, T., Fabert, M., Brevier, J., Habert, R., et al. (2015). Development of a real-time flexible multiphoton microendoscope for label-free imaging in a live animal. *Sci. Rep.* 5, 18303. doi: 10.1038/srep18303

Ferlay, J., Soerjomataram, I., Dikshit, R., Eser, S., Mathers, C., Rebelo, M., et al. (2015). Cancer incidence and mortality worldwide: Sources, methods and major patterns in GLOBOCAN 2012. *Int J Cancer.* 136, E359–E386. doi: 10.1002/ijc.29210

Friedl, P., and Gilmour, D. (2009). Collective cell migration in morphogenesis, regeneration and cancer. *Nat. Rev. Mol. Cell. Biol.* 10, 445–457. doi: 10.1038/nrm2720

Friedl, P., and Wolf, K. (2008). Tube travel: the role of proteases in individual and collective cancer cell invasion. *Cancer Res.* 68, 7247–7249. doi: 10.1158/0008-5472.CAN-08-0784

Green, N. H., Delaine-Smith, R. M., Askew, H. J., Byers, R., Reilly, G. C., Matcher, S. J., et al. (2017). new mode of contrast in biological second harmonic generation microscopy. *Sci. Rep.* 7, 13331. doi: 10.1038/s41598-017-13752-y

Han, X., and Brown, E. (2010). Measurement of the ratio of forward-propagating to back-propagating second harmonic signal using a single objective. *Opt. Express.* 18, 10538–10550. doi: 10.1364/OE.18.010538

Helmchen, F., and Denk, W. (2005). Deep tissue two-photon microscopy. *Nat. Methods* 2, 932–940. doi: 10.1038/nmeth818

Hotary, K., Allen, E., Punturieri, A., Yana, I., and Weiss, S. J. (2000). Regulation of cell invasion and morphogenesis in a three-dimensional type i collagen matrix by membrane-type matrix metalloproteinases 1, 2, and 3. *J. Cell. Biol.* 149, 1309–1323. doi: 10.1083/jcb.149.6.1309

James, D. S., and Campagnola, P. J. (2021). Recent advancements in optical harmonic generation microscopy: applications and perspectives. *BME Front.* 2021, 3973857. doi: 10.34133/2021/3973857

Kauppila, S., Stenbäck, F., Risteli, J., Jukkola, A., and Risteli, L. (1998). Aberrant type I and type III collagen gene expression in human breast cancerin vivo. *J Pathol.* 186, 262–268.

LaComb, R., Nadiarnykh, O., Townsend, S. S., and Campagnola, P. J. (2008). Phase matching considerations in second harmonic generation from tissues: effects on emission directionality, conversion efficiency and observed morphology. *Opt. Commun.* 281, 1823–1832. doi: 10.1016/j.optcom.2007.10.040

Leemans, C. R., Snijders, P. J. F., and Brakenhoff, R. H. (2018). The molecular landscape of head and neck cancer. *Nat. Rev. Cancer*. 18, 269–282. doi: 10.1038/nrc.2018.11

Levental, K. R., Yu, H., Kass, L., Lakins, J. N., Egeblad, M., Erler, J. T., et al. (2009). Matrix crosslinking forces tumor progression by enhancing integrin signaling. *Cell* 139, 891–906. doi: 10.1016/j.cell.2009.10.027

Lu, P., Weaver, V. M., and Werb, Z. (2012). The extracellular matrix: a dynamic niche in cancer progression. *J. Cell. Biol.* 196, 395–406. doi: 10.1083/jcb.201102147

Marur, S., D'Souza, G., Westra, W. H., and Forastiere, A. A. (2010). HPV-associated head and neck cancer: a virus-related cancer epidemic 2010. *Lancet Oncol.* 11:781–789. doi: 10.1016/S1470-2045(10)70017-6

Meyer, T., Guntinas-Lichius, O., Eggeling, F., von Ernst, G., Akimov, D., Schmitt, M., et al. (2013). Multimodal nonlinear microscopic investigations on head and neck squamous cell carcinoma: toward intraoperative imaging. *Head Neck*. 35, E280–E287. doi: 10.1002/hed.23139

Nadiarnykh, O., LaComb, R. B., Brewer, M. A., Campagnola, P. J. (2010). LaComb RB, Brewer MA, Campagnola PJ. Alterations of the extracellular matrix in ovarian cancer studied by Second Harmonic Generation imaging microscopy. *BMC Cancer* 10, 94. doi: 10.1186/1471-2407-10-94

Nelke, K. H., Pawlak, W., Gerber, H., and Leszczyszyn, J. (2014). Head and neck cancer patients' quality of life. *Adv. Clin. Exp. Med.* 23, 1019–1027. doi: 10.17219/acem/37361

Pierik, A. S., Leemans, C. R., and Brakenhoff, R. H. (2021). Resection margins in head and neck cancer surgery: an update of residual disease and field cancerization. *Cancers* 13, 2635. doi: 10.3390/cancers13112635

Poh, C. F., Zhang, L., Anderson, D. W., Durham, J. S., Williams, P. M., Priddy, R. W., et al. (2006). Fluorescence visualization detection of field alterations in tumor margins of oral cancer patients. *Clin Cancer Res*. 12, 6716–6722. doi: 10.1158/1078-0432.CCR-06-1317

Provenzano, P. P., Eliceiri, K. W., Campbell, J. M., Inman, D. R., White, J. G., Keely, P. J., et al. (2006). Collagen reorganization at the tumor-stromal interface facilitates local invasion. *BMC Med*. 4, 38. doi: 10.1186/1741-7 015-4-38

Provenzano, P. P., Inman, D. R., Eliceiri, K. W., Knittel, J. G., Yan, L., Rueden, C. T., et al. (2008). Collagen density promotes mammary tumor initiation and progression. *BMC Med*. 6, 11. doi: 10.1186/1741-7015-6-11

Pupa, S. M., Ménard, S., Forti, S., and Tagliabue, E. (2002). New insights into the role of extracellular matrix during tumor onset and progression. *J. Cell Physiol*. 192, 259–267. doi: 10.1002/jcp.10142

Ramaswamy, S., Ross, K. N., Lander, E. S., and Golub, T. R. (2003). A. molecular signature of metastasis in primary solid tumors. *Nat. Genet*. 33, 49–54. doi: 10.1038/ng1060

Rivard, M., Popov, K., Couture, C.-A., Laliberté M., and Bertrand-Grenier, A., et al. (2014). Imaging the noncentrosymmetric structural organization of tendon with interferometric second harmonic generation microscopy. *J. Biophotonics*. 7, 638–646. doi: 10.1002/jbio.201300036

Rozario, T., and DeSimone, D. W. (2010). The extracellular matrix in development and morphogenesis: a dynamic view. *Dev. Biol*. 341, 126–140. doi: 10.1016/j.ydbio.2009.10.026

Ryser, M. D., Lee, W. T., Ready, N. E., Leder, K. Z., and Foo, J. (2016). Quantifying the dynamics of field cancerization in tobacco-related head and neck cancer: a multiscale modeling approach. *Cancer Res.* 76, 7078–7088. doi: 10.1158/0008-5472.CAN-16-1054

Sapudom, J., Rubner, S., Martin, S., Kurth, T., Riedel, S., Mierke, C. T., et al. (2015). The phenotype of cancer cell invasion controlled by fibril diameter and pore size of 3D collagen networks. *Biomaterials* 52, 367–375. doi: 10.1016/j.biomaterials.2015.02.022

Schindelin, J., Arganda-Carreras, I., Frise, E., Kaynig, V., Longair, M., Pietzsch, T., et al. (2012). Fiji: An open-source platform for biological-image analysis. *Nat. Methods* 9, 676–682. doi: 10.1038/nmeth.2019

Slaughter, D. P., Southwick, H. W., and Smejkal, W. (1953). Field cancerization in oral stratified squamous epithelium; clinical implications of multicentric origin. *Cancer* 6, 963–968.

Sung, H., Ferlay, J., Siegel, R. L., Laversanne, M., Soerjomataram, I., Jemal, A., et al. (2021). Global cancer statistics 2020: GLOBOCAN estimates of incidence and mortality worldwide for 36 cancers in 185 countries. *CA Cancer J. Clin*. 71, 209–249. doi: 10.3322/caac.21660

Tilbury, K., and Campagnola, P. J. (2015). Applications of second-harmonic generation imaging microscopy in ovarian and breast cancer. *Perspect. Medicin. Chem*. 7, 21–32. doi: 10.4137/PMC.S13214

Tilbury, K., Lien, C.-H., Chen, S.-J., and Campagnola, P. J. (2014). Differentiation of Col I and Col III isoforms in stromal models of ovarian cancer by analysis of second harmonic generation polarization and emission directionality. *Biophys. J.* 106, 354–365. doi: 10.1016/j.bpj.2013.10.044

Tilbury, K. B., Campbell, K. R., Eliceiri, K. W., Salih, S. M., Patankar, M., Campagnola, P. J., et al. (2017). Stromal alterations in ovarian cancers via wavelength dependent Second Harmonic Generation microscopy and optical scattering. *BMC Cancer* 17, 102. doi: 10.1186/s12885-017-3090-2

van Houten, V. M. M., Leemans, C. R., Kummer, J. A., Dijkstra, J., Kuik, D. J., van den Brekel, M. W. M., et al. (2004). Molecular diagnosis of surgical margins and local recurrence in head and neck cancer patients: a prospective study. *Clin. Cancer Res*. 10, 3614–3620. doi: 10.1158/1078-0432.CCR-03-0631

Venning, F. A., Wullkopf, L., and Erler, J. T. (2015). Targeting ECM disrupts cancer progression. *Front. Oncol*. 5, 224. doi: 10.3389/fonc.2015.00224

Walker, C., Mojares, E., and Del Río Hernández, A. (2018). Role of extracellular matrix in development and cancer progression. *Int. J. Mol. Sci.* 19, 3028. doi: 10.3390/ijms19103028

Williams, J. C., and Campagnola, P. J. (2015). Wearable second harmonic generation imaging: the sarcomeric bridge to the clinic. *Neuron* 88, 1067–1069. doi: 10.1016/j.neuron.2015.12.009

Williams, R. M., Zipfel, W. R., and Webb, W. W. (2005). Interpreting second-harmonic generation images of collagen I fibrils. *Biophys J*. 88, 1377–1386. doi: 10.1529/biophysj.104.047308

Winn, D. M., Lee, Y.-C., A., Hashibe, M., and Boffetta, P. (2015). The INHANCE consortium: Toward a better understanding of the causes and mechanisms of head and neck cancer. *Oral Dis*. 21, 685–693. doi: 10.1111/odi.12342

Wolf, K., Wu, Y. I., Liu, Y., Geiger, J., Tam, E., Overall, C., et al. (2007). Multi-step pericellular proteolysis controls the transition from individual to collective cancer cell invasion. *Nat. Cell. Biol*. 9, 893–904. doi: 10.1038/ncb1616

Wu, Y., Leng, Y., Xi, J., and Li, X. (2009). Scanning all-fiber-optic endomicroscopy system for 3D nonlinear optical imaging of biological tissues. *Opt. Express*. 17, 7907–7915. doi: 10.1364/OE.17.007907

Yan, J., Zhuo, S., Chen, G., Milsom, J. W., Zhang, H., Lu, J., et al. (2014). Real-time optical diagnosis for surgical margin in low rectal cancer using multiphoton microscopy. *Surg. Endosc*. 28, 36–41. doi: 10.1007/s00464-013-3153-7

Zhang, Y., Akins, M. L., Murari, K., Xi, J., Li, M.-J., et al. (2012). A compact fiber-optic SHG scanning endomicroscope and its application to visualize cervical remodeling during pregnancy. *Proc. Natl. Acad. Sci. U S A*. 109, 12878–12883. doi: 10.1073/pnas.1121495109

Zhang, Z., Munck, J. C., d., Verburg, N., Rozemuller, A. J., Vreuls, W., et al. (2019). Quantitative third harmonic generation microscopy for assessment of glioma in human brain tissue. *Adv. Sci.* 6, 1900163. doi: 10.1002/advs.201900163

Zhu, G.-G., Kauppila, A., Risteli, L., Mäkinen, M., and Stenbäck, F., et al. (1995). Immunohistochemical study of type I collagen and type I pN-collagen in benign and malignant ovarian neoplasms. *Cancer* 75, 1010–1017. doi: 10.1002/1097-0142(19950215)75:4<1010::AID-CNCR2820750417>3.0.CO;2-O

Zipfel, W. R., Williams, R. M., and Webb, W. W. (2003). Nonlinear magic: multiphoton microscopy in the biosciences. *Nat. Biotechnol*. 21, 1369–1377. doi: 10.1038/nbt899